The 1966 "century" flood in Italy: A meteorological and hydrological revisitation

P. Malguzzi,[1] G. Grossi,[2] A. Buzzi,[1] R. Ranzi,[2] and R. Buizza[3]

Received 23 January 2006; revised 6 June 2006; accepted 25 August 2006; published 19 December 2006.

[1] The widespread flood event that affected northeastern and central Italy in November 1966, causing severe damages to vast populated areas including the historical towns of Florence and Venice, is revisited with a modeling approach, made possible by the availability of the ECMWF global reanalysis (ERA-40). A simulated forecasting chain consisting of the ECMWF global model, forcing a cascade of two mesoscale, limited area meteorological models apt to reach a convective resolving scale (about 2 km), is used to predict quantitative precipitation. A hydrological model, nested in the finer-scale meteorological model, is used to reproduce forecasted flood hydrographs for different river basins of the investigated areas. Predicted precipitation is in general very sensitive to initial conditions, especially when associated with convective activity, such as over central Italy, in the Arno river basin. Orographically enhanced precipitation, e.g., the one predicted in the eastern Alps, is quite stable and in good agreement with observations. Hydrological forecasts, made separately in different river basins, reflect the accuracy of the simulated precipitation.

Citation: Malguzzi, P., G. Grossi, A. Buzzi, R. Ranzi, and R. Buizza (2006), The 1966 ''century'' flood in Italy: A meteorological and hydrological revisitation, *J. Geophys. Res.*, *111*, D24106, doi:10.1029/2006JD007111.

1. Introduction

[2] In the period from 3 to 5 November 1966, central and northeastern Italy was affected by a synoptic-scale, severe cyclonic system that caused catastrophic and widespread damages associated with flooding, storm surges and landslides. The most memorable effects were the Arno river flooding in Florence that caused severe losses of artistic heritage, the extreme high water in Venice, and the flooding of the town of Trento (geographical locations are shown in the figures). However, damages and casualties due to flooding and landslides were reported in several areas, including the eastern Alps where the heaviest precipitation was observed.

[3] In Tuscany, the rainfall event was extreme in terms of continuity, intensity, and area coverage [*Ministero dei Lavori Pubblici*, 1970]. The temporal and spatial distribution of precipitation was considered as the ''worst possible'' from the point of view of the hydrological response of the Arno river basin [*De Angelis*, 1969]. Precipitation started around noon of 3 November. During the following night, the Arno water level increased by several meters (six meters in six hours) until the levees were overtopped and broken in different sites. The water reached the Cathedral Square in Florence at around 10 a.m. local time of the following day. In the Arno watershed, highways and railroads were submerged. Only in the evening of 4 November the river water level started to decrease.

[4] Several papers have been published in recent years highlighting mainly meteorological features of this event reconstructed on the basis of global reanalyses. *Soderman et al.* [2003] and *Meneguzzo et al.* [2004], by using the NCEP/NCAR reanalyses to drive directly the limited area model RAMS, examined the sensitivity of the model precipitation in the Arno river basin with respect to model resolution, sea surface temperature, and initiation time. *Bertò et al.* [2004, 2005] applied the backward trajectory method to the ERA-40 fields to study the areas of origin and the transport properties of water vapor in this and other cases of heavy precipitation in the Alps. *De Zolt et al.* [2006] analyzed the sensitivity of the precipitation field using the ERA-40 and NCEP/NCAR reanalyses as initial and boundary conditions for the limited area model BOLAM.

[5] The purpose of this work is to revisit the main features of this extreme event, by exploiting the availability of global reanalysis and of up-to-date meteorological and hydrological prediction models. The aim here is to asses the possibility of a detailed ''hindcast'' (a posteriori forecast) of quantitative precipitation during a severe flood event and of the associated hydrological aspects like river flows, using ''today tools with yesterday data.'' The system implemented for the present investigation simulates a forecast chain, starting from initial conditions derived from the ERA-40 reanalysis. Hereinafter, the word ''forecast'' is used to stress that, for each model run, only data available at the initial condition time are used.

[1] Istituto di Scienze dell'Atmosfera e del Clima, Consiglio Nazionale delle Ricerche, Bologna, Italy.
[2] Department of Civil Engineering, Architecture, Land and Evironment, University of Brescia, Brescia, Italy.
[3] European Centre for Medium-Range Weather Forecasts, Reading, UK.

0148-0227/06/2006JD007111

[6] The event considered here was the most important in Italy in the last century, taking into account its spatial extension and overall intensity. Therefore it represents an ideal test case to evaluate the capability of up-to-date, high-resolution meteorological and hydrological models to predict extreme floods. Such models are becoming more and more useful in the short-range forecasting [*Gouweleeuw et al.*, 2004]. Attention will be focused on the prediction of small-scale features of weather and flood hydrographs, rather than on the prediction of the synoptic, large-scale characteristics of the atmospheric evolution. In particular, emphasis will be put on the verification of predicted precipitation over the whole flooded areas and at the scale of hydrological basins.

[7] The paper is organized as follows. The meteorological analysis of the event is outlined in section 2. The model characteristics and experimental setup are described in section 3. In section 4, the results of the meteorological and hydrological integrations are presented and discussed also in comparison with the aforementioned studies. Finally, the conclusions are drawn in section 5.

2. Meteorological Analysis

2.1. Synoptic Description

[8] The period preceding the event was characterized by the presence of an Atlantic blocking pattern west of the British Isles (Figure 1a), that started collapsing quickly between 1 and 2 November, when a mid tropospheric trough deepened on the eastern flank of the blocking ridge, extending from eastern Europe to Spain (Figure 1b). The trough was reinforced, between 3 and 4 November, by another fast-moving trough coming from the northern Atlantic (Figures 1c and 1d). At the surface, cyclogenesis started over Spain and moved over the western Mediterranean (Figure 1e). A simultaneous intensification of an anticyclone occurred over the Balkans (Figures 1e and 1f). The whole structure appears as a unique amplifying baroclinic wave with westward tilt with height, embedded in a strong large-scale meridional temperature gradient ranging from the Atlantic off of Morocco to the eastern Mediterranean, at latitudes between 30° and 40° N (not shown).

[9] The lowest mean sea level pressure (mslp) over northern Italy at 1200 UTC on 4 November was not very deep (about 994 hPa, see Figure 1f). Nonetheless, the west-to-east pressure gradient over Italy and the Adriatic Sea became very large around this time and was associated with exceptionally strong prefrontal southerly winds. The dramatic intensification of the synoptic-scale zonal gradient of geopotential and mslp, visible in Figures 1d and 1f, respectively, was associated with the formation of a very strong, warm meridional flow to the east of the advancing cold front. This current can be identified with a Warm Conveyor Belt (WCB [*Browning and Roberts*, 1994]) and also with an "atmospheric river" [*Zhu and Newell*, 1998; *Ralph et al.*, 2004], because of the presence of a very large flux of moisture from northern Africa [*Bertò et al.*, 2005].

2.2. Mesoscale Features

[10] On the mesoscale, the evolution of the low-level cyclone appeared to be characterized by multiple pressure minima at 0000 UTC on 4 November (see Figure 2, showing a composite of surface hand-made analyses by *Fea et al.* [1968]), moving northward and embedded in a meridionally elongated trough. A north-south oriented cold front was moving slowly northeastward: the blue line denotes its position 12 hours later. The "warm front" drawn in Figure 2 over the Po Valley actually corresponds to a quasi-stationary boundary that separates the southerly flow from the cold air pool trapped south of the Alps, which is associated with an easterly barrier wind [*Buzzi*, 2005]. Strong radar echoes, indicative of deep convection, were detected roughly at the same time along an almost north-south straight line slightly in advance of the cold front (green spots in Figure 2). *Fea et al.* [1968] report that echo tops reached 11,000 m in the northern half of the convective line. Thunderstorm reports are visible on the weather map in Figure 2 where the northern portion of the convective line intersects the land.

[11] In the first hours of 4 November, the easterly flow over the Po Valley changed into a southerly flow rising over the mountain slope, contributing to strong orographic precipitation. The rapid pressure decrease (see the pressure tendency analysis in Figure 2) reflects the cold air removal. The intense precipitation over the eastern Alps started in association with this regime transition between "blocked flow" at low levels and "flow over." The rising flow over the southern flank of the Alps was nearly moist adiabatic. In this kind of situations, precipitation depends basically on the strength and humidity of the impinging flow, and is therefore more predictable than convective precipitation.

[12] The change in wind regime is illustrated in Figure 3, which shows a time-height cross section of meteorological parameters deriving from the Udine radio sounding station (see location in Figure 4) redrawn from *Fea et al.* [1968]. The period ending at 0000 UTC on 4 November was characterized by a continuous warming, more pronounced at mid tropospheric levels (Figure 3, left). The highest (in time) temperatures were observed at 0000 UTC in a layer between 3 and 4 km, when the freezing level raised up to about 3700 m, starting from a height of about 1500 m on 2 November. Near the surface, the warmest spell was observed around 1200 UTC on 4 November, with temperature rising up to 16°–17°C all along the coast of the northern Adriatic Sea. Saturated or nearly saturated conditions were encountered below 3 km in the entire 2-day period preceding the arrival of the cold front. Figure 3 (right) shows the profiles of wind and specific humidity. The clockwise rotation and intensification with height of the wind vector in the first km above the surface, at 0000 UTC on 4 November, was due to the orographic blocking mentioned above. By 1200 UTC on 4 November the south-south-easterly wind exhibited a maximum speed of 70 knots (35 m/s) at a height between 1500 and 2000 m. At the surface, the maximum intensity of the Sirocco (south-easterly) wind recorded in Venice was 18 m/s at 1500 UTC. Consistently with these observations, the ERA-40 reanalysis shows a wind speed maximum of 32 m/s in the layer between 950 and 850 hPa, with 10 m wind maximum of about 20 m/s over the northern Adriatic Sea.

[13] In summary, the south-easterly wind over the Adriatic, that forced the sea level surge (198 cm in Venice, the highest ever recorded) and the orographic precipitation on the southern flank of the Alps can be considered as the most

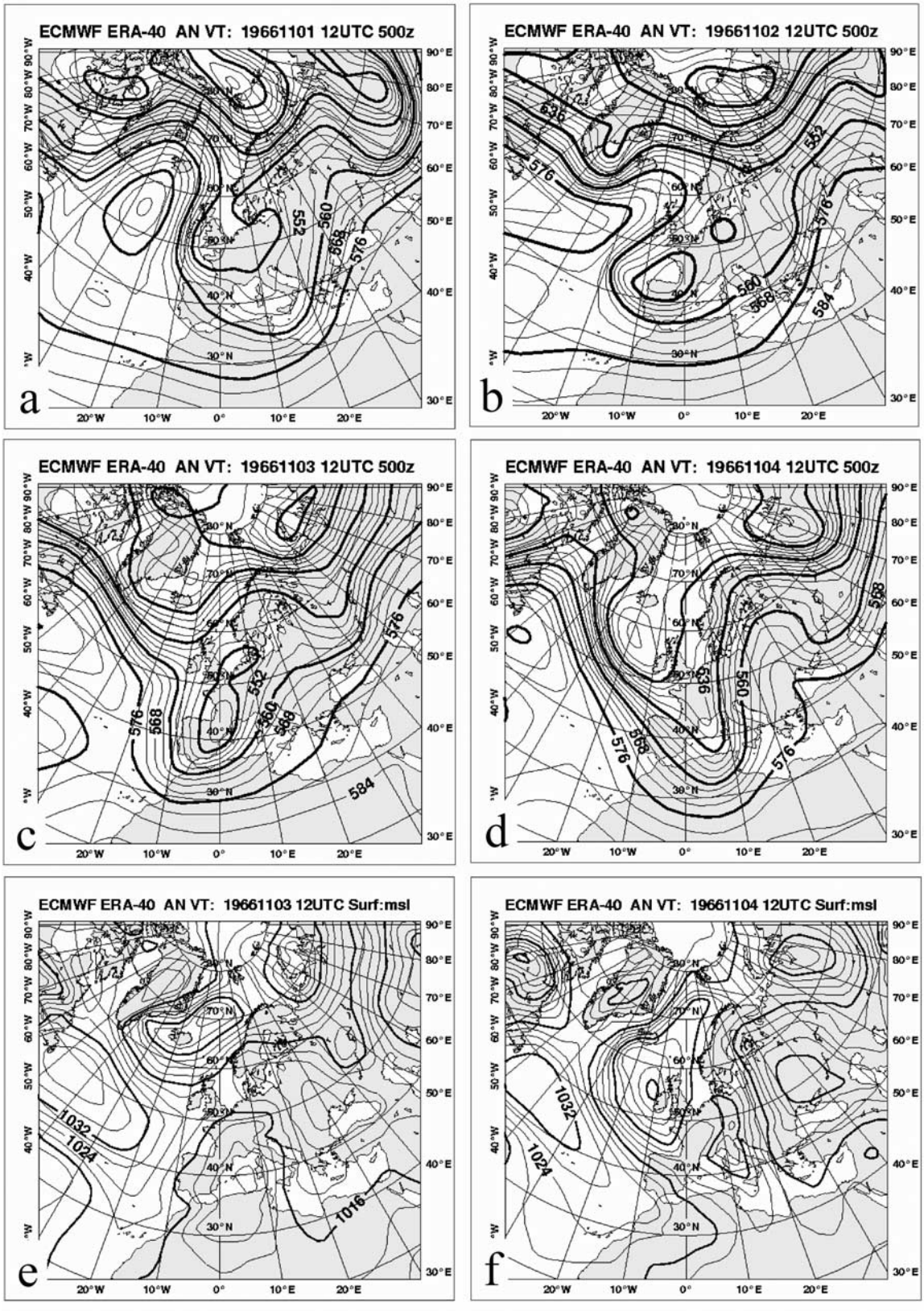

Figure 1. ERA-40 maps (a–d) of geopotential height at 500 hPa (contour interval is 40 m) and (e and f) of mslp (contour interval is 4 hPa). Figure 1a is for 1 November 1966, 1200 UTC; Figure 1b is for 2 November 1966, 1200 UTC; Figures 1c and 1e are for 3 November 1966, 1200 UTC; and Figures 1d and 1f are for 4 November 1966, 1200 UTC.

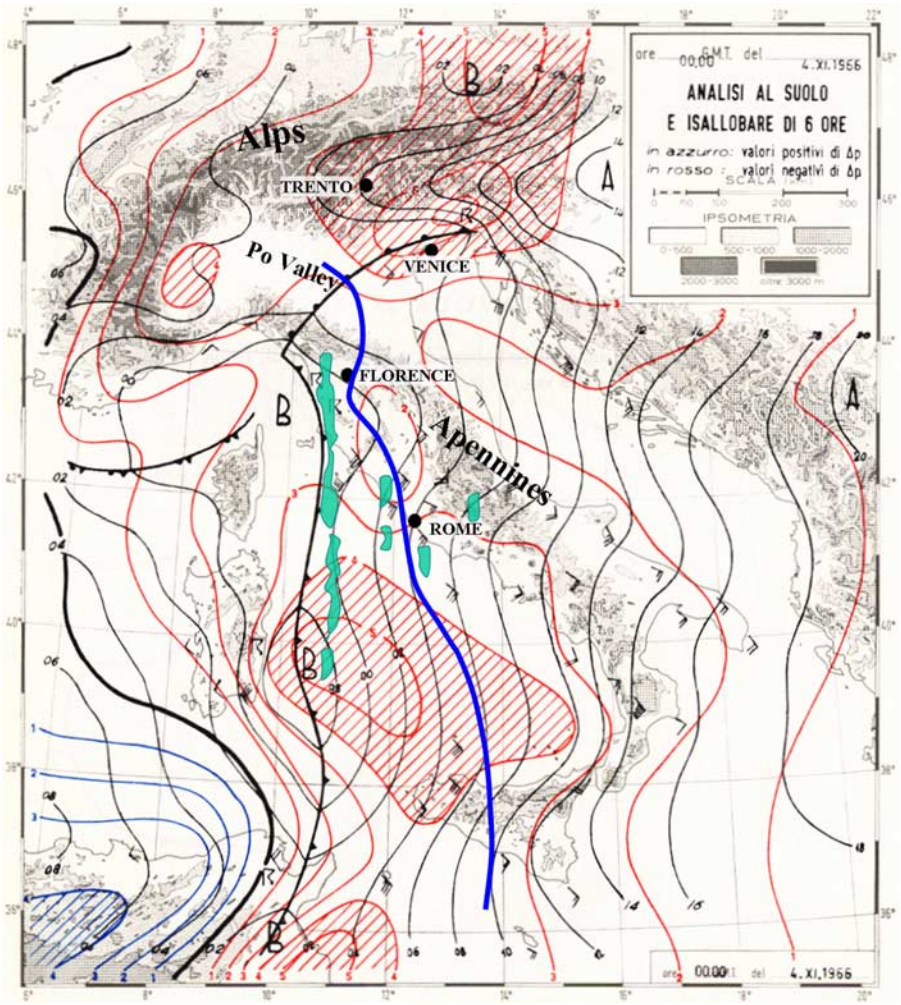

Figure 2. Weather map reelaborated from handmade analyses published by *Fea et al.* [1968]. The basic meteorological fields refer to 4 November 1966, 0000 UTC. Continuous black lines are for mslp, (contour interval 2 hPa). Colored thin lines are for pressure tendency in 6 hours (blue indicates positive, red indicates negative, and contour interval is hPa/6h). Wind barbs are in knots. Low-pressure centers are indicated by B; high pressure is indicated by A. The green spots reproduce reflectivity maxima of the meteorological radar in Rome Fiumicino, at 0040 UTC, same day. The thick blue line indicates the position of the cold front at 1200 UTC of the same day.

relevant atmospheric features characterizing this extreme event. The prefrontal flow, which assumed the character of a strong WCB and of an atmospheric river, was very moist, unstable over central Italy and nearly neutral upstream and over the Alps. It accounted for a very large meridional transport of water vapor. By considering the contribution of the low-level southerly jet in a layer 3 km deep and 200 wide, and by using the specific humidity and wind values reported in Figure 3 at 1200 UTC on 4 November, a flux of water of about 1.2 x 10^8 kg/s impinging over the eastern Alps can be estimated. This value is comparable with that of 1.5 x 10^8 kg/s quoted, for example, by *Ralph et al.* [2004] as typical of atmospheric rivers over the eastern, North Pacific Ocean. For the Alps, during the Mesoscale Alpine Programme (MAP), *Smith et al.* [2003] have estimated an "efficiency" of orographic precipitation of 35%, defined as the ratio between total precipitation rate and incoming vapor flux. This value, though very sensitive to both dynamical and microphysical aspects, allows an estimate of the amount of orographic precipitation that can be produced when an atmospheric river intersects a mountain chain.

2.3. Accumulated Precipitation

[14] The 2-day accumulated precipitation measured at rain gauge stations is presented in Figure 4, superimposed on the precipitation field predicted by one of the high-resolution runs (see the following sections 3 and 4). The analysis is based on a network of 1296 stations, sufficiently dense to resolve mesoscale features of the order of a few tens of km. Original observations were published on the 1966 annual report of the Italian Servizio Idrografico e Mareografico Nazionale [*Ministero dei Lavori Pubblici*, 1970]. The accumulation period of observations spans the time range from 0800 UTC on 3 November to 0800 UTC on 5 November.

[15] Over the eastern Alps an elongated maximum, with several values exceeding 500 mm, extends over the pre-alpine slope, with a well-defined minimum over the Adige

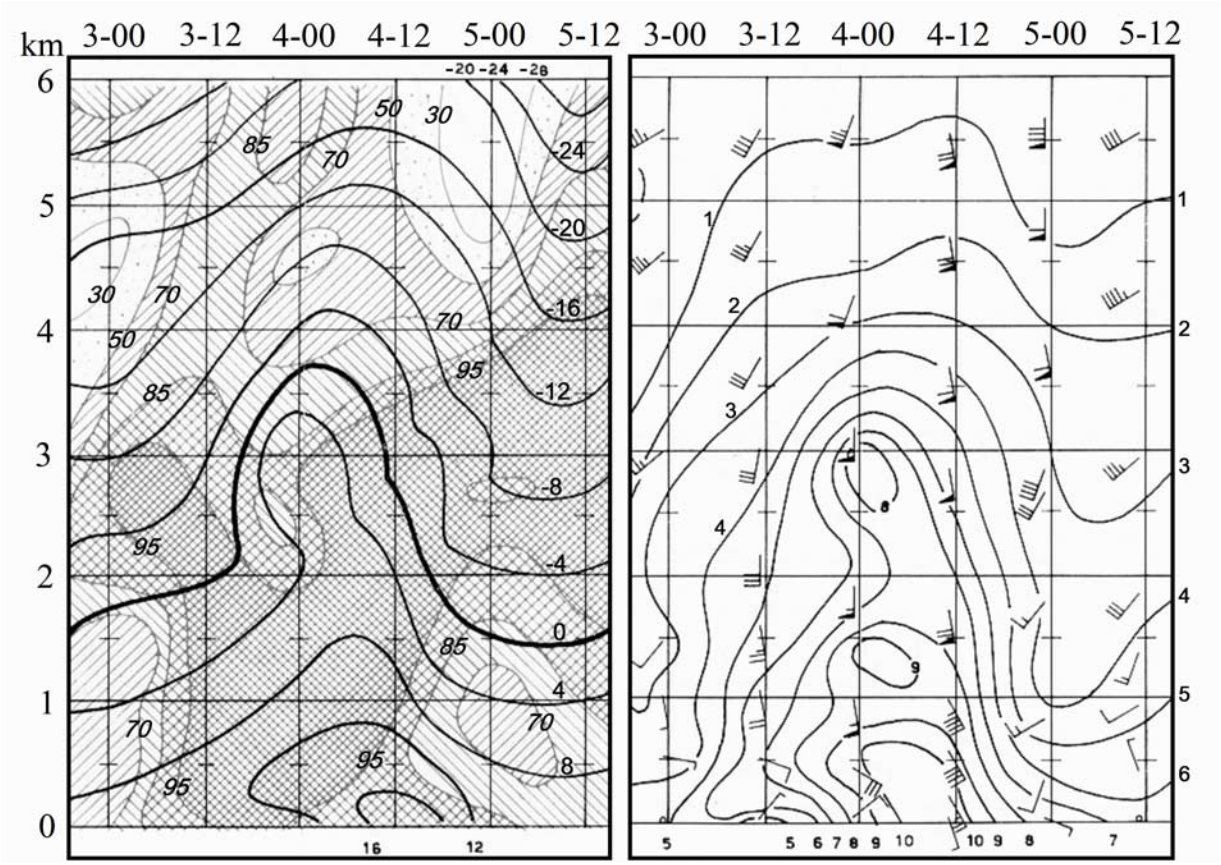

Figure 3. Time (in abscissa, day-UTC hours at the top) and height (in ordinate, from the surface to 6 km) section, based on the Udine (16044) radio-sounding data, every 12 hours, for the period 3 to 5 November 1966, reelaborated from *Fea et al.* [1968]. (left) Temperature (degrees Celsius, thick lines) and relative humidity (hatched). (right) Wind (with conventional symbols, in knots) and specific humidity contours (gr/kg).

valley. The highest value (751 mm in 48 hours) was recorded in the station of Barcis. Large precipitation amounts, in the range 200–400 mm, were also observed further north, at the alpine divide. Severe flooding affected all the main rivers from the Adige catchment to the east, including the Drau river north of the main crest. At most of the streamflow stations and artificial reservoirs, river level records and discharges were the highest ever recorded since the end of the 19th century. Up to 2 $m^3/s/km^2$ of runoff peak were recorded in basins as large as 2000 km^2, and more than 2 $m^3/s/km^2$ for basins of 400 km^2 in size. Precipitation in the alpine region was due mainly to the orographic uplift, in stable or neutral (moist) conditions.

[16] The other main flooding area, corresponding to the Arno and Ombrone rivers, is characterized by a well-defined precipitation band, with values in excess of 300 mm in 2 days, which extends from the Tyrrhenian coast toward northeast, where the springs of the Arno river are located. Up to 1.2 $m^3/s/km^2$ of runoff peak were recorded in the Ombrone river at Sasso d'Ombrone, gauging an area of 2657 km^2, and the specific flood peak of the Arno river at Subbiano, gauging an area of 738 km^2 in size, was about 3 $m^3/s/km^2$. As anticipated in the previous subsection, there is evidence both from SYNOP and radar observations (see Figure 2), that deep convection contributed to this precipitation maximum. A secondary maximum is observed upstream and above the northern Apennine divide, partly in the Sieve river basin, tributary of the Arno river. This maximum is clearly due to an orographic forcing, although it is not possible to separate the contribution of convection to the total precipitation fallen in this area. Floods, though less severe than in Tuscany, also affected rivers flowing north of the Apennines.

3. Models and Methodology

3.1. Meteorological Models

[17] The initial conditions for the European Centre Medium-Range Weather Forecasts (ECMWF) global prediction model, used in the present study, were taken from the T_L159L60 (where 159 is the horizontal spectral truncation and 60 the number of vertical levels) ERA-40 reanalysis, having the horizontal resolution corresponding to roughly 130 km along a meridian. It should be recalled that in 1966 there were no satellite and very few aircraft data, while the number of conventional data was within a factor of two from the number available today [*Simmons and Gibson*, 2000; *Uppala*, 2001; *Uppala et al.*, 2005]. This has clearly an impact on the quality of ERA-40 analysis. Considering, for example, 1-day forecasts for the 500 hPa geopotential

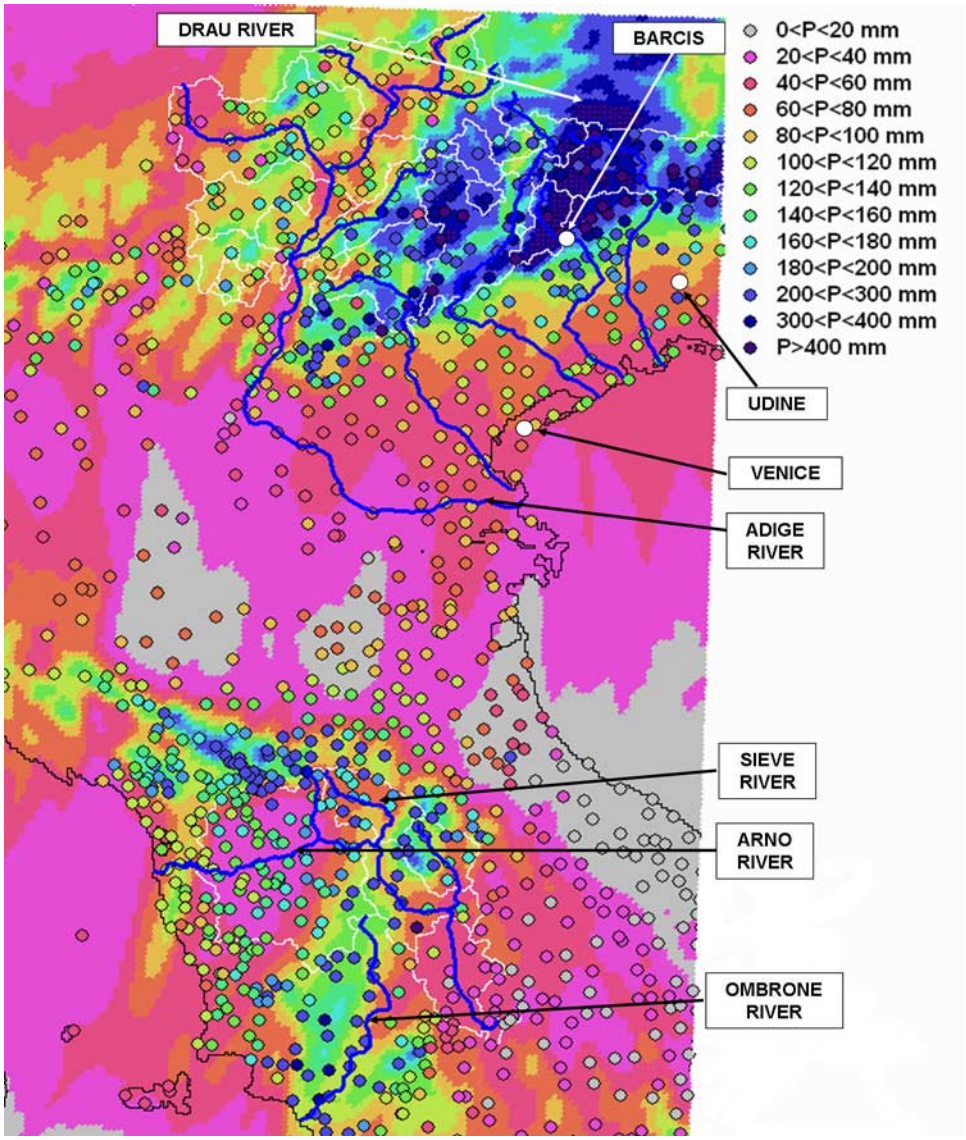

Figure 4. Observed 48 hour accumulated rainfall (circles) in the period ending 5 November 1966, 0800 UTC, superimposed over the precipitation field produced by MOLOCH for Exp3CONV (see text). The blue lines represent the major rivers described in the paper; white lines represent the major watershed divides.

height over the northern hemisphere, *Uppala et al.* [2005] report that the average error of forecasts started between 1958 and 1960 is about 40% larger than the error of forecasts started between 1989 and 1991.

[18] A series of forecasts of the ECMWF global spectral model with resolution $T_L511L60$ were performed starting at different initial condition times. This model version (cycle 23r4) was used operationally at ECMWF between 12 June 2001 and 22 January 2002 [see *Simmons*, 2001; *Uppala et al.*, 2005]. In cascade, high-resolution, limited area meteorological forecasts have been made using the one-way, multiple nesting technique, having as initial and boundary conditions the fields derived from the ECMWF forecasts. A large downscaling factor (about 60 in the present case) is needed, since the hydrological applications to small size basins, typical of the area under investigation, require a few km resolution precipitation fields. With this approach it is tested the capability of a purely dynamical downscaling, in the assumption that small scales can be consistently reconstructed from the large-scale atmospheric dynamical features, and by prescribing the appropriate topographic forcing.

[19] The limited area models used in this study are BOLAM and MOLOCH, both developed at ISAC-CNR. BOLAM [*Buzzi et al.*, 1994] is a meteorological model based on the primitive equations in hydrostatic approximation. It uses sigma coordinates and wind components, potential temperature, specific humidity, surface pressure, and concentration of five hydrometeor classes as dependent variables, distributed on a nonuniformly spaced Lorenz grid. The horizontal discretization uses geographical coordinates, with latitudinal rotation on the Arakawa C-grid. The model implements a "Weighted Average Flux" (WAF [*Billet and Toro*, 1997]) scheme for the three-dimensional

Table 1. Initial Conditions for the Meteorological Forecast Chain[a]

Experiments	ECMWF, T511, L60, Global	BOLAM_18, 18 km, L38, 27 × 27°	BOLAM_6, 6 km, L44, 11 × 11°	MOLOCH, 2.2 km, L50, 4 × 6.6°
Exp1CONV	2 Nov 0000 UTC	2 Nov 0000 UTC	3 Nov 0600 UTC, conv.	3 Nov 0700 UTC
Exp1NOCONV	···	···	3 Nov 0600 UTC, no conv.	3 Nov 0700 UTC
Exp2CONV	2 Nov 1200 UTC	2 Nov 1200 UTC	3 Nov 0600 UTC, conv.	3 Nov 0700 UTC
Exp2NOCONV	···	···	3 Nov 0600 UTC, no conv.	3 Nov 0700 UTC
Exp3CONV	3 Nov 0000 UTC	3 Nov 0000 UTC	3 Nov 0600 UTC, conv.	3 Nov 0700 UTC
Exp3NOCONV	···	···	3 Nov 0600 UTC, no conv.	3 Nov 0700 UTC

[a]Horizontal grid spacing, number of vertical levels, and the size of the integration domain are reported for each meteorological model.

advection. The lateral boundary conditions are imposed using a relaxation scheme that minimizes wave energy reflection. A detailed description of the dynamics and numerical schemes is given by *Buzzi and Foschini* [2000]. The water cycle for stratiform precipitation is described by means of a simplified approach similar to that proposed by *Schultz* [1995]. Deep convection is parameterized using the Kain-Fritsch convective scheme [*Kain and Fritsch*, 1990; *Kain*, 2004]. The surface and boundary layer parameterization is based on the *E-l* approximation, in which turbulent kinetic energy is predicted explicitly. Surface processes consist in the water and energy balance in a three-layer ground model. The atmospheric radiation is computed with a combined application of the Geleyn [*Ritter and Geleyn*, 1992] and ECMWF scheme [*Morcrette*, 1991; *Mlawer et al.*, 1997]. The initial and boundary variables are obtained by interpolating the atmospheric, surface, and ground variables from the ECMWF model forecasts to the higher-resolution BOLAM grid.

[20] MOLOCH is a nonhydrostatic, convection-resolving model. It integrates the fully compressible set of equations with prognostic variables (pressure, temperature, specific humidity, horizontal and vertical velocity components, and five water species) represented on the lat-lon rotated, Arakawa C-grid. Terrain following coordinates, relaxing smoothly to horizontal surfaces away from the earth surface, are employed. Model dynamics are integrated in time with an implicit scheme for the vertical propagation of sound waves, while explicit, time-split schemes are implemented for the remaining terms. Three-dimensional advection is computed using the eulerian WAF scheme. Horizontal fourth-order diffusion and divergence damping are included to prevent energy accumulation on the shorter space scales. The physical scheme consists of radiation (as for BOLAM), subgrid turbulence, microphysics, and soil water and energy balance. The turbulence scheme is based on an *E-l* closure, where the turbulent kinetic energy equation (including advection) is evaluated. Surface turbulent fluxes of momentum, specific humidity, and temperature are computed by the classical Monin-Obukhov theory with Businger/Holtslag functions in the unstable/stable case. The mixing length is computed from turbulent kinetic energy [*Deardorff*, 1980] in the stable atmosphere and from *Bougeault and Lacarrere* [1989], modified by *Zampieri* [2004], in the unstable environment. The microphysical scheme is based on the parameterization proposed by *Drofa and Malguzzi* [2004]. The physical processes determining the time tendency of specific humidity, cloud water/ice and precipitating water/ice are divided into ''fast'' and ''slow'' ones. Fast processes involve transformations between specific humidity and cloud quantities and are computed every advection time step. Temperature is updated by imposing exact entropy conservation at constant pressure. Fall of precipitation is computed with the stable and dispersive backward-upstream scheme, with fall velocities depending on concentration. The soil scheme used here is similar to the one of BOLAM. MOLOCH is nested into the BOLAM runs performed at coarser resolution.

[21] The period of interest for the meteorological and hydrological forecasting has been identified in the 48 hour time span from 0800 UTC on 3 November to 0800 UTC on 5 November 1966. This covers almost the entire precipitation period and corresponds to the rain gauge accumulation interval of 2 days (ending each day at 0800 UTC). This constraint has determined the forecast interval for the highest-resolution meteorological model. The total forecast time, considering the initial time of the global ECMWF model, has been varied in the range between 54 and 78 hours. This allows the assessment of forecast quality as a function of the forecast duration.

[22] Table 1 shows the initial condition times for each model run, the model grid spacing being indicated in the first row. There is roughly a downscaling factor of 3 between consecutive nesting steps. The domain extension in lat-lon degrees is also indicated. The MOLOCH domain is elongated in latitude to embrace the two main precipitation areas. Boundary condition updating is performed every 3 hours for BOLAM_18 (18 km grid spacing), every 1.5 hours for BOLAM_6, and every hour for MOLOCH.

[23] At 6 km, BOLAM tends to produce explicit convective precipitation with unrealistic spatial scales. Existing parameterization schemes are not meant to work properly at such a high resolution, because of the fact that there is no clear scale separation between subgrid and explicitly represented convection [*Kain*, 2004; *Warner and Hsu*, 2000]. The inner MOLOCH model does not have this problem, since it is capable of representing convection explicitly. When the 6 km model parameterizes convection, the inflow atmospheric profiles tend to be more stable, therefore decreasing the potential for development of convection by the nonhydrostatic inner model. In the opposite case, i.e., without convective parameterization in the outer domain, errors due to the misrepresentation of convective scales can adversely affect the inner domain simulation through boundary condition influence. Since there is no general remedy to this problem, except enlarging the inner domain as much as possible, it was decided to perform, for each experiment, two different runs of BOLAM_6, with and without activation of the parameterization of convection (named, respectively, ''CONV'' and ''NOCONV'' in

Table 1). Therefore six 2.2 km forecasts and associated input precipitation fields are available for the hydrological model.

3.2. Hydrological Model

[24] The hydrological model employed here (DIMOSOP) is a conceptual distributed model, previously used to simulate past flood events [*Bacchi et al.*, 2002; *Bacchi and Ranzi*, 2003] and to produce real-time forecasts in the Toce river basin (Piedmont, northwestern Italy) during the MAP Special Observing Period [*Ranzi et al.*, 2003; *Grossi and Kouwen*, 2004]. The conceptual scheme adopted to estimate the rainfall partitioning into interception, runoff and infiltration is the Curve Number Method, widely investigated by the U.S. Soil Conservation Service [see *U.S. Department of Agriculture*, 1986], and successfully tested in several Italian basins. It assumes that the storm runoff volume is proportional, at each computational time step, to the rainfall volume exceeding a threshold, through the ratio between the accumulated infiltration and the soil water storage capacity. The threshold represents initial water losses mainly due to depression storage and interception. The flood routing process is represented through a dynamic Muskingum-Cunge scheme, solving the linear parabolic convection-diffusion equation. Different hydraulic parameters are used to discriminate overland and channel flow, as described by *Ranzi et al.* [2002].

[25] For the Arno case, the topography was obtained from a 250x250m Digital Elevation Model (DEM). This DEM was used to automatically extract the river network that determines the flood routing. The parameters describing the river channel geometry were assumed on the basis of surveys on the investigated basins, as reported by *Orlandini and Rosso* [1998]. The time lag in some sub basins of the Arno river was derived from the application of the pioneering mathematical model of *Natale and Todini* [1977]. The soil hydrological properties and the storage capacity parameter were derived, using the standard procedures suggested by U.S.D.A., from the permeability and land use maps provided by the Arno Water Authority. The permeability values were quite in agreement with other maps of soil hydraulic properties produced for some selected areas in the Arno basin [see *Becchi et al.*, 1995].

4. Results and Discussion

4.1. Meteorological Forecasts

[26] In this section the focus is put on the validation of the precipitation fields. The ECMWF precipitation (Figure 5) and the corresponding MOLOCH precipitation (Figure 6), accumulated over the period of interest, are presented for all the experiments listed in Table 1. MOLOCH precipitation of Exp3CONV, with convective parameterization activated in the BOLAM_6 run, is also plotted in Figure 4 using the same palette as observed data, in order to facilitate the comparison between predictions and observations.

[27] The ECMWF model is able to predict the two main precipitation spots over the Alps and near the Tyrrhenian side of Central Italy in all the forecasts. With reducing forecast validity, the position of precipitation centers tends to be more correctly located but with strong underestimation of maxima, especially over the Alpine region. The forecast starting at 0000 UTC on 2 November (Figure 5a) shows a very broad precipitation pattern over the Alps, with a maximum of about 255 mm and a secondary maximum of 190 mm over the northwestern part of Tuscany. However, the main precipitation band over central-southern Tuscany is totally missed. The highest value over the eastern Alps, in excess of 300 mm, is predicted starting at 2 November, 1200 UTC (Figure 5b), while the maximum over Tuscany is shifted toward the correct position but with weak intensity. The last forecast experiment (Exp. 3, Figure 5c) predicts more accurately the position of the Tuscany maximum, though the precipitation amount is still underestimated. The same holds for the Alpine maximum, which is more precisely located with respect to the earlier starting forecasts.

[28] The corresponding high-resolution precipitation fields (Figure 6), although reflecting the much more detailed scales of the orography and of the convective dynamics, show overall similar features in terms of changes of the initial conditions. The precipitation amount and spatial distribution over the Alps are definitely more realistic, although the absolute maximum varies between an underestimation of 673 mm (Exp3CONV) and an overestimation of 1050 mm (Exp2, both CONV and NOCONV), as a function of the initial condition time. Over Tuscany, there is still an underestimation of the total precipitation but, at variance with ECMWF forecasts, strong precipitation upstream of the Apennines, in the catchment area of the Arno river, is now forecasted. In particular, in Exp. 3 (Figures 6e–6f) the two separate maxima over Tuscany appear in the correct position. Over the Po Valley, north of the Apennines, observations show an area of relatively weak precipitation around 50 mm. This indicates that no important convective precipitating system occurred over this region. The high-resolution model catches this feature, though the precipitation amounts in the lee (north) of the Apennines are generally underestimated. In summary, the high-resolution meteorological fields produced by Exp3 (CONV and NOCONV) give the best results. Inspection at Figure 4 reveals a good agreement between observed and predicted precipitation in the northeastern Alpine region, in terms of both 1 maximum locations and precipitation amounts. Over Tuscany, the main rainfall band with predicted precipitation amounts over 200 mm is well located, but underestimated when compared to the observed values, which are in excess of 300 mm.

[29] Similar conclusions can be drawn by inspection of Figure 7, which shows a scatter diagram of predicted versus observed accumulated precipitation, integrated over several river basins and relative subbasins located in Tuscany and northern Italy (see also next subsection). The points enclosed by circles are relative to Arno subbasins and major tributaries, whose geographical location is shown in Figure 8. It can be seen that over the alpine river basins (their watershed divides are marked by white lines in Figure 4) there is no systematic error, while precipitation over the Arno river is, on average, underpredicted. It can be noticed, in particular, the underestimation over the Sieve river basin.

[30] Observed (and predicted) precipitation timing is closely associated with the movement of the frontal line from west to east and to the corresponding low-level southerly jet (WCB), as discussed in section 2. The forecast

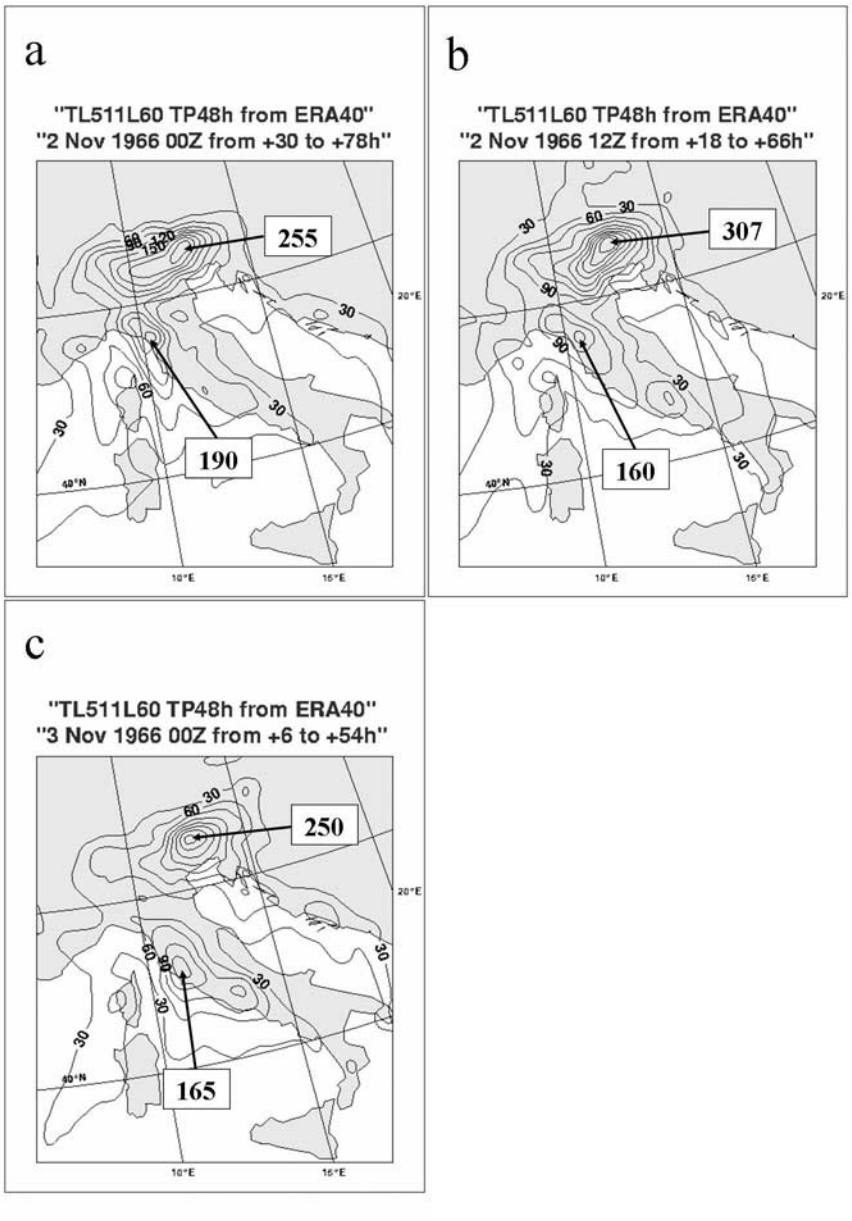

Figure 5. The 48 hour accumulated precipitation, in the period ending 5 November 1966, 0600 UTC, for the ECMWF forecasts (see text) starting (a) 2 November 0000 UTC, (b) 2 November 1200 UTC, and (c) 3 November 0000 UTC. Contour interval is 30 mm. Precipitation maxima in the two main areas are reported.

of the frontal propagation turns out to be sensitive to the time of the initial condition. In general, the lower-resolution models tend to overestimate the frontal speed (not shown). This, in turn, implies a reduction of precipitation amounts predicted over central Italy by the higher-resolution models.

[31] The aforementioned publications by *Soderman et al.* [2003] and *Meneguzzo et al.* [2004] allow only a qualitative intercomparison between the precipitation fields obtained with the high-resolution models over Tuscany, because of the different setup conditions and initialization times, and because of the use of NCEP/NCAR reanalyses in place of global forecasts. Broadly speaking, the precipitation distributions and amounts simulated in the above-mentioned papers are comparable with those of MOLOCH Exp.3. *De Zolt et al.* [2006], by contrasting the precipitation simulations based on the different (ECMWF and NCEP/NCAR) analyses, show that differences are associated with visible discrepancies between the two data sets. In particular, the simulation based on NCEP/NCAR reanalysis seems more accurate in reproducing the main precipitation band over the Ombrone river.

[32] Concerning the MOLOCH predictions with and without convective parameterization activated in the BOLAM_6 runs, the main differences are noticed, as expected, in the areas where convective activity develops, namely over the Tyrrhenian Sea and central Italy. These

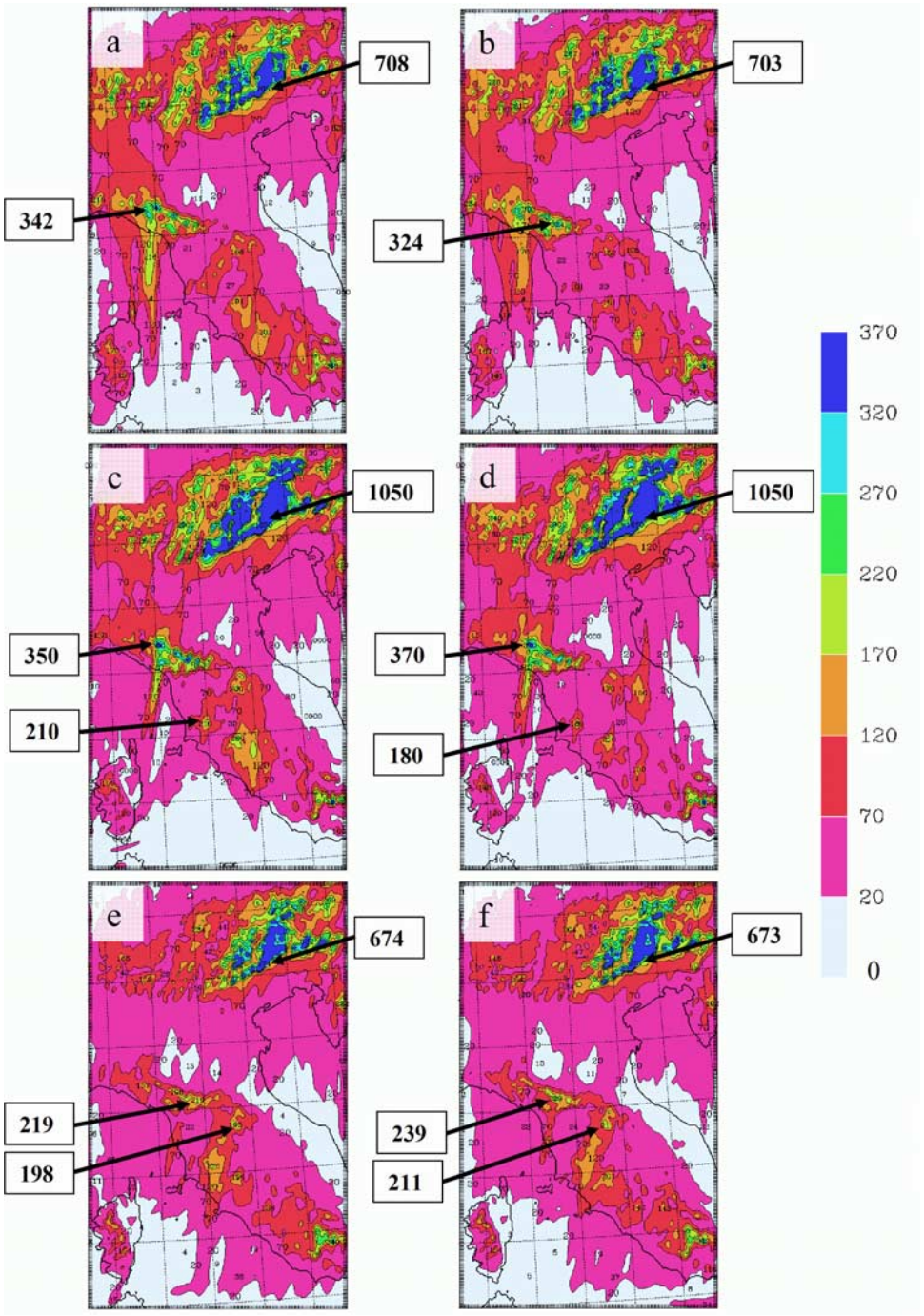

Figure 6. The 47 hour accumulated precipitation, in the period ending 5 November 1966, 0600 UTC, for the six MOLOCH forecasts nested in the BOLAM forecasts reported in Table 1: (a) Exp1NOCONV, (b) Exp1CONV, (c) Exp2NOCONV, (d) Exp2CONV, (e) Exp3NOCONV, and (f) Exp3CONV. Contour interval is 30 mm. The main precipitation maxima are indicated.

areas are located just downstream, with respect to the mean tropospheric flow, the boundaries where the properties of the inflow depend on the activation of convective parameterization in the BOLAM_6 model. In such areas, precipitation at 2.2 km is, on average, slightly larger in the NOCONV experiments. Because of the presence of explicit convective cells in the MOLOCH runs, the rainfall patterns are anisotropic, being elongated in the direction of cell propagation. In the CONV experiments, the explicit convective cells in MOLOCH initiate later, i.e., downstream and farther away from the southwestern boundaries, because of the more stable inflow profiles. This effect, however, does not extend north of the Apennines. Over the alpine region the precipitation pattern and intensity is hardly affected by the switch of parameterized convection in the driving model, suggesting that orographic uplift is the main mechanism for precipitation formation in that area.

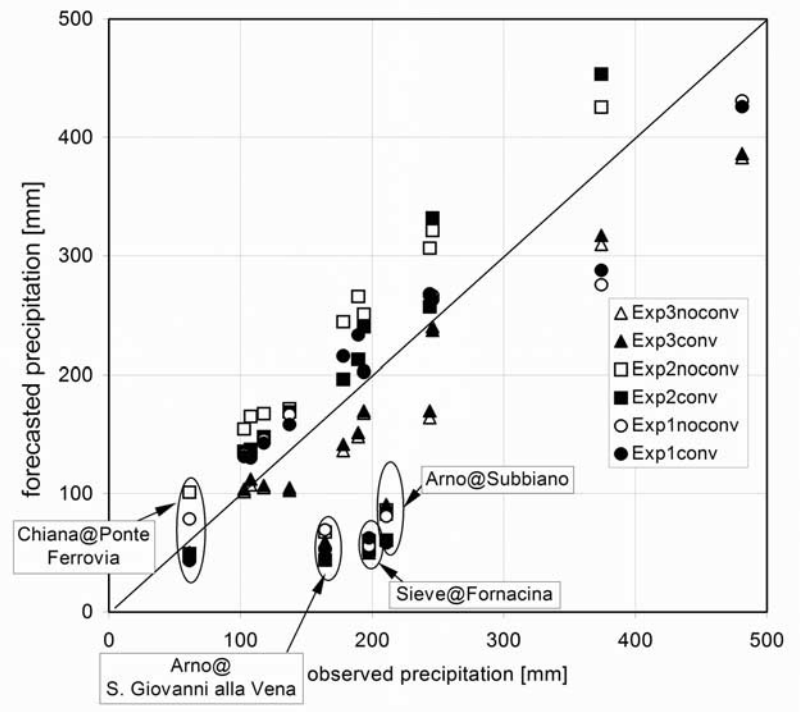

Figure 7. Observed and forecasted total precipitation (48 hours) in the Arno river basins and in some alpine basins delineated in Figure 4.

4.2. Hydrological Forecasts

[33] The precipitation fields produced by MOLOCH were used to force the DIMOSOP hydrological model in order to reproduce the flood hydrograph at the sections of the Arno river and of its main tributaries shown in Figure 8. Flood predictions were done also for most of the subbasins, outlined in Figure 4, in the Alpine area. Only results obtained with Exp3 (CONV or NOCONV) are presented here since, as shown in the previous subsection, this experiment gives the best prediction from the meteorological point of view.

[34] It is notable that MOLOCH at 2.2 km computes the precipitation field at a spatial resolution much higher than the density of rain gauges. In fact, while most of the rain gauges working at the time of the event provided daily amounts, only a subset recorded the rainfall time series continuously. In order to check separately the validity of the hydrological model, a ''control'' run was first performed for each basin, using the hourly precipitation time series recorded by the gauges available within the basin itself. Areal precipitation was computed by implementing a Thiessen interpolation procedure; the same procedure, in practice a nearest-neighbor interpolation, was applied to distribute the forecasted precipitation fields. No calibration of the hydrological and hydraulic parameters was done after the initial model setup.

[35] For the Arno watershed, the complete observed hydrograph was actually available for the section of the Arno river at S.Giovanni alla Vena and for the section of the Sieve river at Fornacina. For the other river sections, only the peak discharge and part of the flood hydrographs (generally the rising limb) were recorded before the flood damaged the instrumentation. Results are shown here for the Fornacina closure section only (see in Figure 9 the complete hydrograph). The control run shown in Figure 9 is satisfactory in reproducing the ascending and descending part of the hydrograph, as well as the total runoff volume and peak discharge values, but does not reproduce the plateau in the observed hydrograph. This is probably due to the fact that the few recording rain gauges (only 6 gauges reported hourly precipitation over the Sieve basin) were not completely representative of the rainfall area distribution. The ''upside-down hyetograph'' shows rain rate time series averaged over the basin area. As shown in Figure 7 for the river Sieve at Fornacina, the differences between the CONV and NOCONV experiments are very small. In both cases, the timing of maximum precipitation intensity is good, but the peak duration is too short. Concerning predicted hydrographs, the shape of their evolution is quite similar to the control case, although the underestimation of precipitation intensity, before and after the maximum, induces an underestimation of runoff volumes and discharge peaks at the closure section.

[36] The discrepancy between predictions and observations is lower for the wider area of the Arno river at S. Giovanni alla Vena (not shown), which is less sensitive to the errors in the spatial location of precipitation maxima. In fact, the geomorphology and soil characteristics of the Arno watershed suggest that the main tributes to the flood in Florence came from the Sieve river basin at Fornacina (837 km^2) and the upper Arno river basin closed at the section of Subbiano (738 km^2). In the precipitation field of both the Exp3CONV and Exp3NOCONV experiments, the precipitation maximum, which occurred in part in the Sieve

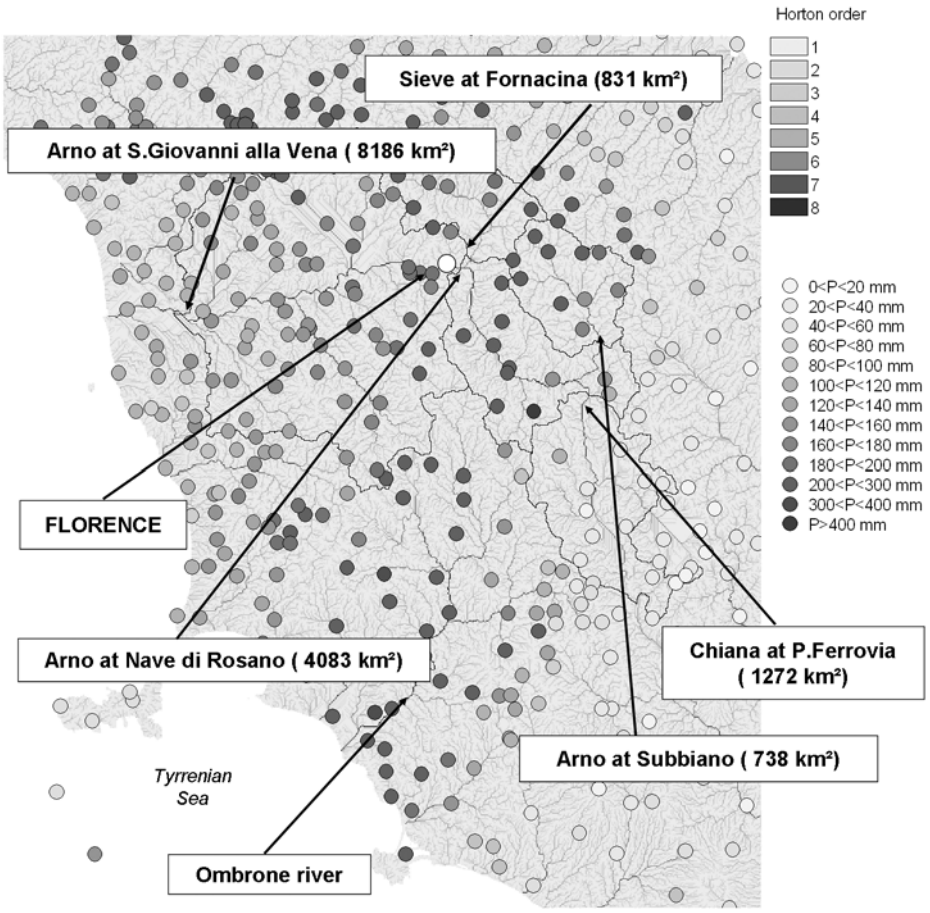

Figure 8. River network derived from the 250 m Arno basin DEM. Horton orders of river channels are represented. Watershed divides of major subbasins are reported.

area, is shifted in the northeast direction. Therefore the Sieve discharge underestimation is compensated by an overestimation in the upper Arno basin.

[37] Figure 10 reports a scatterplot showing control and forecasted versus observed peak flows over several river basins located in Tuscany and in the Alps, obtained from the Exp3CONV. This diagram shows that the peak flows are well reproduced in the control runs in both areas, while the forecasted peaks are well reproduced in the alpine basins but underestimated in Tuscany, where the precipitation was

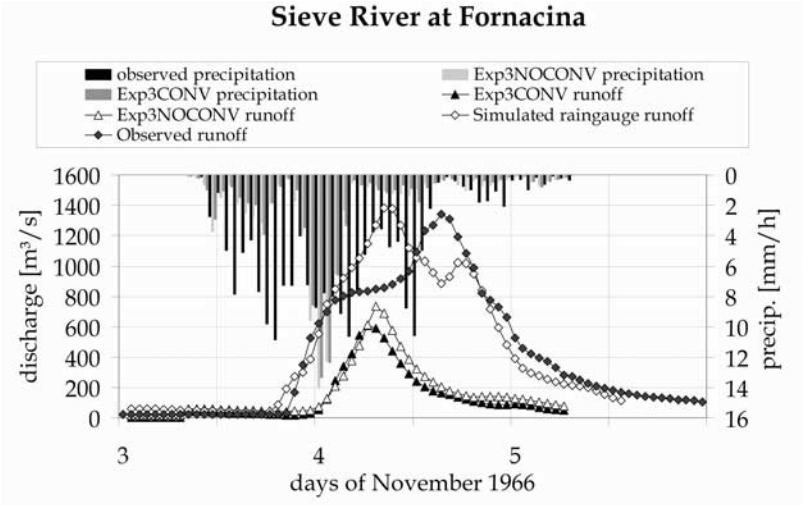

Figure 9. Observed and forecasted flood hydrograph for the Sieve river at the section of Fornacina. Forecasted precipitation is from Exp3.

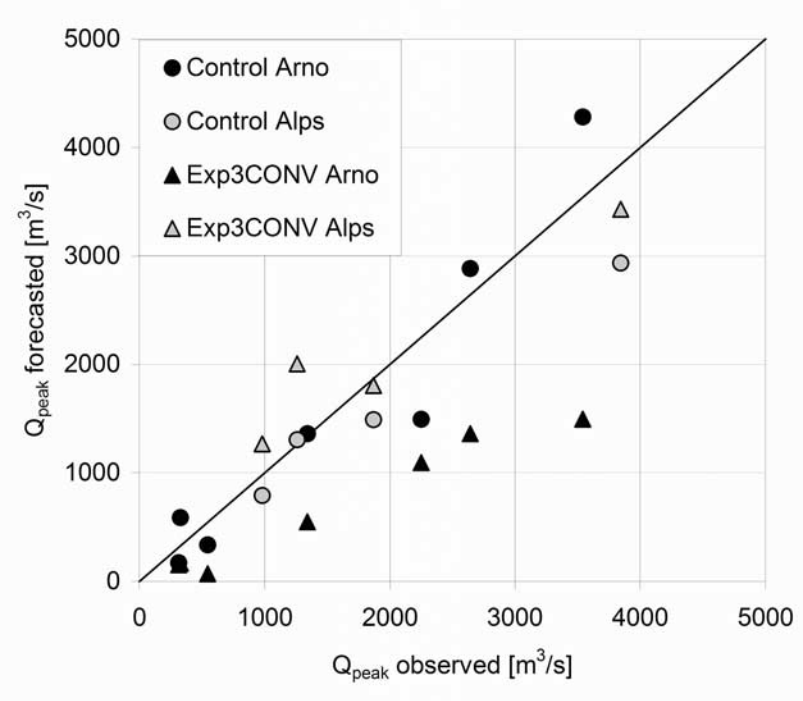

Figure 10. Scatter diagram of control/forecasted versus observed flow peaks for the Arno river and alpine basins. Different points correspond to different subbasins or different closure sections. Forecasted precipitation is from Exp3CONV.

mainly of convective type. In Figure 10, only the monitored sections upstream of Florence are reported, since the discharge observed at S. Giovanni alla Vena was strongly affected by breaches in the river levees and by the flooding of the area around and, especially, downstream the city of Florence. Exp3NOCONV (not shown) gives similar results.

[38] Figure 11 shows the results of the hydrological control run and of the flood forecast in the small (392 km^2 in size) Cellina river basin at Barcis, in the eastern Alps, in the area where the maximum precipitation was measured. In this case, the control and forecasted flood hydrographs for the Exp3CONV experiment reproduce well the observations, both in terms of timing and discharge peak, while the total volume is slightly overpredicted. This hydrograph is representative of other results obtained for the Alpine area [see also *Ranzi et al.*, 2004]. Also for this case, Exp3NOCONV (not shown) gives similar results.

5. Conclusions

[39] A meteohydrological forecasting chain was set up to simulate the catastrophic flood that caused severe damages and loss of lives in several areas of Italy in early November 1966. This experiment was performed by nesting the non-hydrostatic MOLOCH model into the hydrostatic BOLAM, limited area meteorological model, in turn driven by the ECMWF global forecasts initialized with the ERA-40 reanalysis. With the resolution of 2.2 km of the inner MOLOCH model, small-scale spatial and temporal details of the meteorological fields relevant for the flood generation can be simulated. The DIMOSOP conceptual distributed hydrological model was employed to forecast hydrographs and discharge peaks, starting from the predicted high-resolution precipitation.

[40] The quality of the meteorological forecast chain depends not only from the model characteristics, but also from the accuracy of the ERA40 reanalysis. In the period considered, the reanalysis quality is negatively affected by

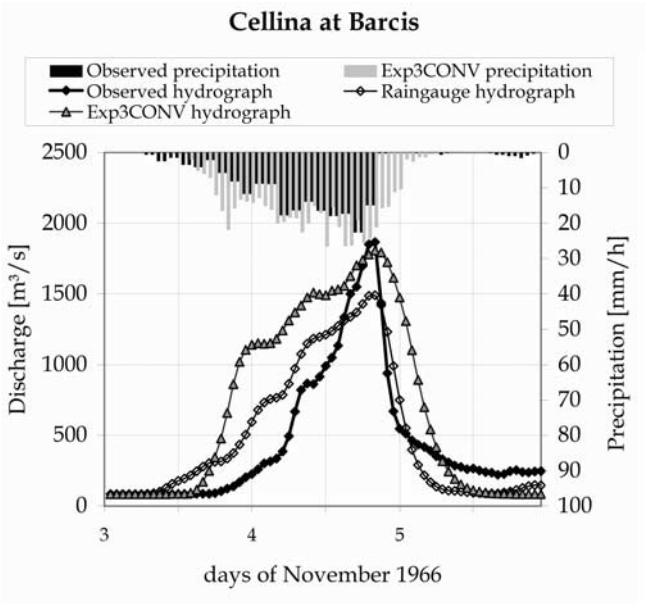

Figure 11. Observed and forecasted flood hydrograph for the Cellina river at the section of Barcis. Forecasted precipitation is from Exp3CONV.

the absence of satellite data, which nowadays represent a basic source of information especially over oceanic regions. The data coverage dishomogeneity, when moving from the Atlantic ocean to continental Europe, can partly explain the degradation of the forecasts with increasing validity time, considering that the large-scale disturbance responsible for this event was generated over the Atlantic. Only the forecast starting at 0000 UTC on 3 November provided useful precipitation fields over the Tuscany area, where precipitation was mainly of convective type. Nevertheless, good forecasts of the exceptionally intense orographic precipitation over the eastern alpine region could be obtained with more than 48 hours in advance, as shows by Figure 6.

[41] The high-resolution nonhydrostatic simulations were nested into intermediate-resolution hydrostatic runs performed with and without convective parameterization. The experiments described in section 4 showed that, although the BOLAM runs without parameterization of convection presented some important underestimation of precipitation amounts in the convective areas over central Italy, the impact on the MOLOCH results remained small, as indicated for example by the scatter diagram of Figure 7, and by the hydrographs of Figure 9. It would be erroneous, however, to draw general conclusions from inspection of a single case.

[42] The 48 hours accumulated observed precipitation, averaged over several subbasins in the northeastern Alps and in the area of the Arno river, was compared with the corresponding predicted fields. The ground truth verification shows a general agreement, in the alpine area, of the forecasted fields initialized from 48 to 24 hours before the onset of the precipitation event. Concerning the Tuscany area, the timing of the forecasted precipitation is accurate, but the total amount is well reproduced only for the northern and southern part of the Arno basin, and is underestimated in the other major upstream tributaries and downstream over areas close to the basin outlet, measuring about 8,000 km^2 in size.

[43] Regarding the estimate of the forecast usefulness in terms of flood warnings, it can be concluded that with the meteohydrological model chain here implemented, and with the meteorological observations available in 1966, an effective flood warning 24 to 48 hours in advance of the flood peak, that occurred in the afternoon of 4 November, could have been issued for the alpine region. However, for the Tuscany area, including the Arno river basin, realistic amounts of precipitation could only be predicted in advance of about 24 hours, and even that with important local underestimations. Therefore, for the latter area, a timely warning based purely on model tools could only have been issued from 12 to 18 hours in advance of the precipitation peak, and about 24 hours before the flood peak.

[44] **Acknowledgments.** The Arno River Water Authority is acknowledged for the permeability and land use maps provided. The Pisa branch of the hydrographic service is thanked for having provided some hydrometric data.

References

Bacchi, B., and R. Ranzi (2003), Hydrological and meteorological aspects of floods in the Alps: An overview, *Hydrol. Earth. Syst. Sci.*, *7*(6), 785–798.

Bacchi, B., G. Grossi, R. Ranzi, and A. Buzzi (2002), On the use of coupled mesoscale meteorological and hydrological models for flood forecasting in midsize mountain catchments: operational experience and verification, in *Proceedings of the 2nd International Symposium on Flood Defence, Beijing, China, September 10–13, 2002*, vol. II, edited by Wu et al., pp. 965–972, Sci. Press, New York.

Becchi, I., E. Caporali, L. Castellani, and E. Palmisano (1995), Hydrological control of flooding: Tuscany, October 1992, *Surv. Geophys.*, *16*, 227–252.

Bertò, A., A. Buzzi, and D. Zardi (2004), Studio della perturbazione meteorologica responsabile della piena dell'Adige nel 1966 mediante analisi di traiettorie lagrangiane paper presented at XXIX Convegno Nazionale di Idraulica e Costruzioni Idrauliche, Univ. degli Studi di Trento, Trento, Italy, 7–10 Sept.

Bertò, A., A. Buzzi, and D. Zardi (2005), A warm conveyor belt mechanism accompanying extreme precipitation events over north-eastern Italy, *Hrv. Meteorol. Casopis*, *40*, 338–341.

Billet, S., and E. F. Toro (1997), On WAF-type schemes for multidimensional hyperbolic conservation laws, *J. Comput. Phys.*, *130*, 1–24.

Bougeault, P., and P. Lacarrere (1989), Parameterisation of orography-induced turbulence in a mesoscale model, *Mon. Weather Rev.*, *117*, 1872–1890.

Browning, K. A., and N. Roberts (1994), Structure of a frontal cyclone, *Q. J. R. Meteorol. Soc.*, *120*, 1535–1557.

Buzzi, A. (2005), Heavy precipitation and Alpine orography paper presented at International Workshop on Timely Warnings of Heavy Precipitation Episodes and Flash Floods, Slovenian Meteorol. Soc., Ljubljana, Slovenia, 21–22 Oct.

Buzzi, A., and L. Foschini (2000), Mesoscale meteorological features associated with heavy precipitation in the southern alpine region, *Meteorol. Atmos. Phys.*, *72*, 131–146.

Buzzi, A., M. Fantini, P. Malguzzi, and F. Nerozzi (1994), Validation of a limited area model in cases of Mediterranean cyclogenesis: Surface fields and precipitation scores, *Meteorol. Atmos. Phys.*, *53*, 137–153.

De Angelis, G. (1969), *Le acque dell'Arno*, Editrice Itinerari, Lanciano, Italy.

Deardorff, J. W. (1980), Stratocumulus-capped mixed layers derived from a three dimensional model, *Boundary Layer Meteorol.*, *18*, 495–527.

De Zolt, S., P. Lionello, P. Malguzzi, A. Nuhu, and A. Tomasin (2006), The effect of the boundary conditions on the simulation of the 4 November 1966 storm over Italy, *Adv. Geosci.*, *7*, 199–204.

Drofa, O. V., and P. Malguzzi (2004), Parameterisation of microphysical processes in a non-hydrostatic prediction model, paper presented at 14th International Conference on Clouds and Precipitation, World Meteorol. Organ., Bologna, Italy, 19–23 July.

Fea, G., A. Gazzola, and A. Cicala (1968), Prima documentazione generale della situazione meteorologica relativa alla grande alluvione del novembre 1966, *CNR-CENFAM PV, 32*, 215 pp., Cons. Naz. delle Ric., Rome.

Gouweleeuw, B., P. Reggiani, and A. De Roo (2004), A European flood forecasting system EFFS. Full report of the EFFS project, funded under the FPV research programme of the European Commission, 304 pp., Inst. for Environ. and Sustainability, Joint Res. Cent., Ispra, Italy.

Grossi, G., and N. Kouwen (2004), Intercomparison among hydrologic simulations coupled to meteorological predictions provided by different mesoscale meteorological models, paper presented at XXIX Convegno di Idraulica e Costruzioni Idrauliche, Univ. degli Studi di Trento, Trento, Italy, 7–10 Sept.

Kain, J. S. (2004), The Kain-Fritsch convective parameterisation: An update, *J. Appl. Meteorol.*, *43*, 170–181.

Kain, J. S., and J. M. Fritsch (1990), A one-dimensional entraining/detraining plume model and its application in convective parameterization, *J. Atmos. Sci.*, *47*, 2784–2802.

Meneguzzo, F., M. Pasqui, G. Menduni, G. Messeri, B. Gozzini, D. Grifoni, M. Rossi, and G. Maracchi (2004), Sensitivity of meteorological high-resolution numerical simulations of the biggest floods occurred over the Arno river basin, Italy, in the 20th century, *J. Hydrol.*, *288*, 37–56.

Ministero dei Lavori Pubblici (1970), *Annali Idrologici—1966, Bologna, Parma, Pisa, Roma, Venezia*, Ist. Poligrafico dello Stato, Rome.

Mlawer, E. J., S. J. Taubman, P. D. Brown, M. J. Iacono, and S. A. Clough (1997), Radiative transfer for inhomogeneous atmospheres: RRTM, a validated correlated-k model for the longwave, *J. Geophys. Res.*, *102*(D16), 663–682.

Morcrette, J.-J. (1991), Radiation and cloud radiative properties in the ECMWF operational weather forecast model, *J. Geophys. Res.*, *96*, 9121–9132.

Natale, L., and E. Todini (1977), A constrained parameter estimation technique for linear models in hydrology, in *Mathematical Models for Surface Water Hydrology*, edited by T. A. Ciriani, U. Maione, and J. R. Wallis, pp. 109–147, John Wiley, Hoboken, N. J.

Orlandini, S., and R. Rosso (1998), Parameterization of stream channel geometry in the distributed modeling of catchment dynamics, *Water Resour. Res.*, *34*(8), 1971–1985.

Ralph, F. M., P. J. Neiman, and G. A. Wick (2004), Satellite and CALJET aircraft observations of atmospheric rivers over the eastern North Pacific Ocean during the winter of 1997/98, *Mon. Weather Rev.*, *132*, 1721–1745.

Ranzi, R., M. Bochicchio, and B. Bacchi (2002), Effects on floods of recent forestation and urbanisation in the Mella River (Italian Alps), *Hydrol. Earth Syst. Sci.*, *6*(2), 239–265.

Ranzi, R., B. Bacchi, and G. Grossi (2003), Runoff measurements and hydrological modelling for the estimation of rainfall volumes in an alpine basin, *Q. J. R. Meteorol. Soc.*, *129*, 653–672.

Ranzi, R., R. Buizza, A. Buzzi, and P. Malguzzi (2004), Previsione e controllo di eventi idrologici estremi: l'alluvione del novembre 1966 nel Triveneto, paper presented at XXIX Convegno di Idraulica e Costruzioni Idrauliche, Univ. degli Studi di Trento, Trento, Italy, 7–10 Sept.

Ritter, B., and J. F. Geleyn (1992), A comprehensive radiation scheme for numerical weather prediction models with potential applications in climate simulations, *Mon. Weather Rev.*, *120*, 303–325.

Shultz, P. (1995), An explicit cloud physics parameterisation for operational numerical weather prediction, *Mon. Weather Rev.*, *123*, 3331–3343.

Simmons, A. J. (2001), Development of the ERA-40 data assimilation system, *ECMWF Reanal. Proj. Rep. Ser.*, *3*, pp. 11–31, Eur. Cent. for Med.-Range Weather Forecasts, Reading, U. K.

Simmons, A. J., and J. K. Gibson (2000), The ERA-40 project plan, *ECMWF Reanal. Proj. Rep. Ser.*, *1*, 62 pp., Eur. Cent. for Med.-Range Weather Forecasts, Reading, U. K.

Smith, R. B., Q. Jiang, M. G. Fearon, P. Tabary, M. Dorninger, J. D. Doyle, and R. Benoit (2003), Orographic precipitation and air mass transformation: An Alpine example, *Q. J. R. Meteorol. Soc.*, *129*, 433–454.

Soderman, D., et al. (2003), Very high resolution precipitation forecasting on low cost high performance computer systems in support of hydrological modeling, paper presented at 17th Conference on Hydrology, AMS Annual Meeting, Am. Meteorol. Soc., Long Beach, Calif., 9–13 Feb. (Available at http://www.ametsoc.org/AMS)

Uppala, S. (2001), ECMWF Re-analysis 1957–2001, ERA-40, *ECMWF Reanal. Proj. Rep. Ser.*, 3, pp. 1–11, Eur. Cent. for Med.-Range Weather Forecasts, Reading, U. K.

Uppala, S. M., et al. (2005), The ERA-40 reanalysis, *Q. J. R. Meteorol. Soc.*, *131*, 2961–3012.

U.S. Department of Agriculture (1986), Urban hydrology for small watersheds, *Tech. Release 55*, Nat. Resour. Conserv. Serv., Washington, D. C.

Warner, T., and H.-M. Hsu (2000), Nested-model simulation of moist convection: The impact of coarse-grid parameterized convection on fine-grid resolved convection, *Mon. Weather Rev.*, *128*, 2211–2231.

Zampieri, M. (2004), Comparison among first, second and third order CBL model, paper presented at 16th Symposium on Boundary Layers and Turbulence, Am. Meteorol. Soc., Portland, Maine.

Zhu, Y., and R. E. Newell (1998), A proposed algorithm for moisture fluxes from atmospheric rivers, *Mon. Weather Rev.*, *126*, 725–735.

R. Buizza, European Centre for Medium-Range Weather Forecasts, Reading RG2 9AX, UK.

A. Buzzi and P. Malguzzi, Istituto di Scienze dell'Atmosfera e del Clima, Consiglio Nazionale delle Ricerche, I-40129 Bologna, Italy. (p.malguzzi@isac.cnr.it)

G. Grossi and R. Ranzi, DICATA, University of Brescia, I-25121 Brescia, Italy.